International Journal of Solids and Structures 96 (2016) 380–392

Contents lists available at ScienceDirect

International Journal of Solids and Structures

journal homepage: www.elsevier.com/locate/ijsolstr

On spatial aliasing in the phononic band-structure of layered composites

A.B.M. Tahidul Haque, Jongmin Shim*

Department of Civil, Structural, and Environmental Engineering, University at Buffalo, Buffalo, NY, USA

ARTICLE INFO

Article history:
Received 12 August 2015
Revised 28 April 2016
Available online 24 May 2016

ABSTRACT

The conventional finite element (FE) method has been used to efficiently obtain phononic dispersion relations for a wide range of geometries and materials. The motive of this research is to draw attention to the research community and addressing that special care should be taken in interpreting the FE results of dispersion analysis for some periodic structures whose FE model possesses an artificial periodicity. Layered composites have been investigated as a representative example to study this numerical issue. Despite the simple geometry of layered composites, it is well known that the accuracy of numerical dispersion relations for waves perpendicular to the layers may be highly impaired by the existence of fictitious modes. The spectral distortion stems from an arbitrarily selected unit cell which causes an artificial finite periodicity in the direction parallel to the composite layers, and they are known to be highly dependent on the unit cell configuration. However, this issue has never been thoroughly investigated, and there has been no specific guideline for a proper unit cell configuration for numerical dispersion relations. In this study, using the classical analytical solution for wave motion in the sagittal plane, the authors show that the spectral distortion induced from the artificial finite periodicity are the manifest results of spatial aliasing in the wavevector domain. In order to prevent the spectral distortion in numerical dispersion relations for waves perpendicular to the layers, this study presents a definitive guideline based on an anti-aliasing condition and the effective elastic modulus theory for layered composites and demonstrates its validity.

Published by Elsevier Ltd.

1. Introduction

The conventional finite element (FE) method has been adopted to efficiently obtain phononic dispersion relations for a wide range of geometries and materials: dispersion relations of homogeneous medium (Babaee et al., 2015a; Bertoldi and Boyce, 2008b; Guarin-Zapata and Gomez, 2015; Han et al., 2016; Langlet et al., 1995; Nelson and Navi, 1975; Ungureanu et al., 2016), dispersion relations of layered composites (Aberg and Gudmundson, 1997; Guarin-Zapata and Gomez, 2015; Minagawa et al., 1981; Naciri et al., 1994), 2-D periodic medium's dispersion relations in the out-of-plane direction (Bertoldi and Boyce, 2008a; 2008b; Li et al., 2009), 2-D periodic medium's dispersion relations in the in-plane direction (Bayat and Gordaninejad, 2014; 2015; Liu and Gao, 2007; Mousanezhad et al., 2015; Shim et al., 2015; Spadoni et al., 2009; Wang et al., 2013; Xu et al., 2012; Zhang et al., 2016), 3-D periodic medium's dispersion relations (Babaee et al., 2015b; Li et al., 2008, 2012; 2013; Wang and Bertoldi, 2012), etc. In the last few years, several researchers have been also investigating the effect of nonlinearities on phononic dispersion relations in the conventional FE framework (Babaee et al., 2015b; Bayat and Gordaninejad, 2014; Mousanezhad et al., 2015; Shim et al., 2015; Wang and Bertoldi, 2012; Wang et al., 2013). For the sake of clarity, we would like to briefly review how the dispersion analysis is typically performed to see the effect of nonlinearities in the community. In general, the analysis is executed in a two-step manner. In the first step, static analysis is performed on an infinitely-periodic structure subjected to external loading. Because this first step is standard static analysis, material and geometric nonlinearities can be easily considered in the conventional FE framework. Secondly, on the deformed structure (at the end of the first analysis) as the base configuration, wave propagation analysis (i.e., eigenvalue analysis) is executed to calculate the dispersion relations of the deformed structure. This second step in nature is linear perturbation analysis. In this two-step manner, researchers have been investigating the evolution of the dispersion relations of various structures, and they found that

* Corresponding author. Department of Civil, Structural, and Environmental Engineering, University at Buffalo, Buffalo, NY, USA
E-mail address: jshim@buffalo.edu (J. Shim).

http://dx.doi.org/10.1016/j.ijsolstr.2016.05.014
0020-7683/Published by Elsevier Ltd.

material and geometric nonlinearities affect phononic band-gaps (Babaee et al., 2015b; Bayat and Gordaninejad, 2014; Mousanezhad et al., 2015; Shim et al., 2015; Wang and Bertoldi, 2012; Wang et al., 2013).

Despite the above mentioned versatility of the conventional FE method, the motive of this research is to draw attention to the research community and addressing that special care should be taken in interpreting dispersion relations obtained in the conventional FE framework. For the dispersion relations of layered composites, it is well-known that some numerical techniques cause fictitious modes affected by the geometry of an arbitrarily chosen unit-cell (e.g., FE method in Aberg and Gudmundson (1997); Guarin-Zapata and Gomez (2015); Minagawa et al. (1981); Naciri et al. (1994), variational method in Minagawa and Nemat-Nasser (1977)). On the other hand, to obtain the dispersion relations of homogeneous medium (Babaee et al., 2015a; Bertoldi and Boyce, 2008b; Guarin-Zapata and Gomez, 2015; Han et al., 2016; Langlet et al., 1995; Nelson and Navi, 1975; Ungureanu et al., 2016) and 2-D periodic medium's dispersion relations in the out-of-plane direction (Bertoldi and Boyce, 2008a; 2008b; Li et al., 2009), an artificial periodicity was arbitrarily introduced in the conventional FE framework. However, researchers are not even aware of the possibility of the fictitious modes in the numerically obtained dispersion relations. In the community working on wave finite element (WFE) method (Mace and Manconi, 2008; Manconi, 2008), these spurious branches in the dispersion relations of composite medium have been investigated and a solution to the numerical issue has been also proposed. However, in the community adopting the conventional FE method for dispersion analysis, there has been no report investigating the origin of this spectral distortion. Thus, we considered layered composites as a representative example to study the origin of the spectral distortions.

Layered composites have been widely adopted for various applications including thermal conductivity controllable materials (Lee et al., 1997; Pernot et al., 2010), tunable piezoelectric materials (Wang et al., 2014) and nano-structured polymer layers (Cheng et al., 2008). In particular, wave propagation in layered composites has been an interesting subject in engineering mechanics, so many aspects of the problem have been analytically investigated. For instance, the analytical dispersion relations of layered composites have been obtained for several limiting cases such as elastic wave propagation perpendicular to the layers (He et al., 1988; Lee and Yang, 1973), parallel to the layers (Sun et al., 1968b) and both parallel and perpendicular to the layers (Brekhovskikh, 1980; Rytov, 1956). Moreover, these studies have significantly contributed to the emergence of innovative materials for acoustic waveguide (Saini et al., 2011) and acoustic rectifier (Liang et al., 2010).

In parallel with analytical studies, several numerical approaches have been introduced to investigate wave motion of various types of periodic composites. Numerical techniques for obtaining phononic dispersion relations include the continuum power series method (Hegemier and Bache, 1974; Hegemier and Nayfeh, 1973), the effective stiffness method (Herrmann and Achenbach, 1967; Sun et al., 1968a), the mixture theory (Murakami, 1985; Murakami and Akiyama, 1985; Murakami et al., 1979), the plane wave expansion method (Zhao and Wei, 2009), the finite difference method (Mukherjee and Lee, 1978), the variational method (Kohn et al., 1972; Nemat-Nasser, 1972) and the conventional FE method (Aberg and Gudmundson, 1997). All these numerical techniques provide dispersion relations for mechanical waves propagating within layered composites.

However, despite the simple geometry of layered composites (shown in Fig. 1A), the results of some numerical techniques (including the conventional FE method) for phononic dispersion relations for wave propagation perpendicular to the layers should be carefully interpreted. It is well known that the accuracy of numerical analysis is highly impaired by the existence of fictitious modes (Aberg and Gudmundson, 1997; Guarin-Zapata and Gomez, 2015; Minagawa and Nemat-Nasser, 1977; Minagawa et al., 1981; Naciri et al., 1994). It is obvious that structural 1-D elements (e.g., truss or beam elements) are not suitable for the analysis of layered composites. In order to model layered composites in a 1-D setting in the conventional FE framework, one needs an element having an infinite length in the direction parallel to the layers (i.e., x_1 direction in Fig. 1A) and a finite length in the direction perpendicular to the layers (i.e., x_3 direction). However, all the commercial FE software (e.g., ABAQUS, COMSOL, ANSYS, LS-DYNA, etc.) offers infinite elements in 2-D or 3-D settings, which have intrinsic finite length-scale along the x_1 direction. Thus, it is not possible to model layered composites in the ideal 1-D setting in the conventional FE framework. Instead, in the research community, a 2-D setting under the plane strain condition has been generally employed together with a periodic boundary condition in both directions (i.e., x_3 as well as x_1). Furthermore, this constraint is not limited to the conventional FE method. For example, a variational method employed in Minagawa and Nemat-Nasser (1977) also suffers the same limitation, and the dispersion analysis of layered composites are obtained in a 2-D setting using a rectangular unit cell in 2-D space. For instance, Fig. 1D illustrates numerical dispersion relations calculated in the conventional FE framework, and it shows some wave modes (marked by solid lines) which are not expected from the corresponding analytical solution in Fig. 1C. The appearance of those fictitious modes are known to be highly affected by the aspect ratio of the selected unit cell for the considered layered composites (Aberg and Gudmundson, 1997; Guarin-Zapata and Gomez, 2015; Minagawa and Nemat-Nasser, 1977; Minagawa et al., 1981; Naciri et al., 1994). In order to avoid the spectral distortion, just a thin unit cell is suggested to be employed. However, this issue has never been thoroughly investigated in the community adopting the conventional FE method for dispersion analysis, and there has been no specific guideline for a proper unit cell configuration for numerical dispersion relations.

Therefore, for wave propagation perpendicular to the layers, the objectives of this study is to systematically investigate the origin of spectral distortion in numerical dispersion relations obtained in the conventional FE framework and to provide a definitive guideline to exclude those fictitious modes for a frequency range of interest. Through this study, we remind that special care should be taken in interpretation dispersion relations obtained in the conventional FE framework. In order to achieve these objectives, we first re-visit the analytical dispersion relations for coupled in-plane waves (so-called sagittal waves) in layered composites. Then, the analytical approach is employed to identify the origin of the fictitious modes in dispersion relations for wave propagation perpendicular to the layers. Furthermore, for a frequency range of interest, we suggest a specific guideline for a proper unit cell configuration and demonstrate the soundness of the suggestion.

2. Method of analysis

It is widely known that sampling a continuous signal at discrete but equally spaced instants of time causes fictitious frequencies in the corresponding spectral domain due to the act of discretization. This spectral distortion is called temporal aliasing, and it occurs when a discrete Fourier series is employed for approximating a continuous periodic function (Newland, 1993). Temporal aliasing is a well-known issue in signal processing, and it can be avoided if

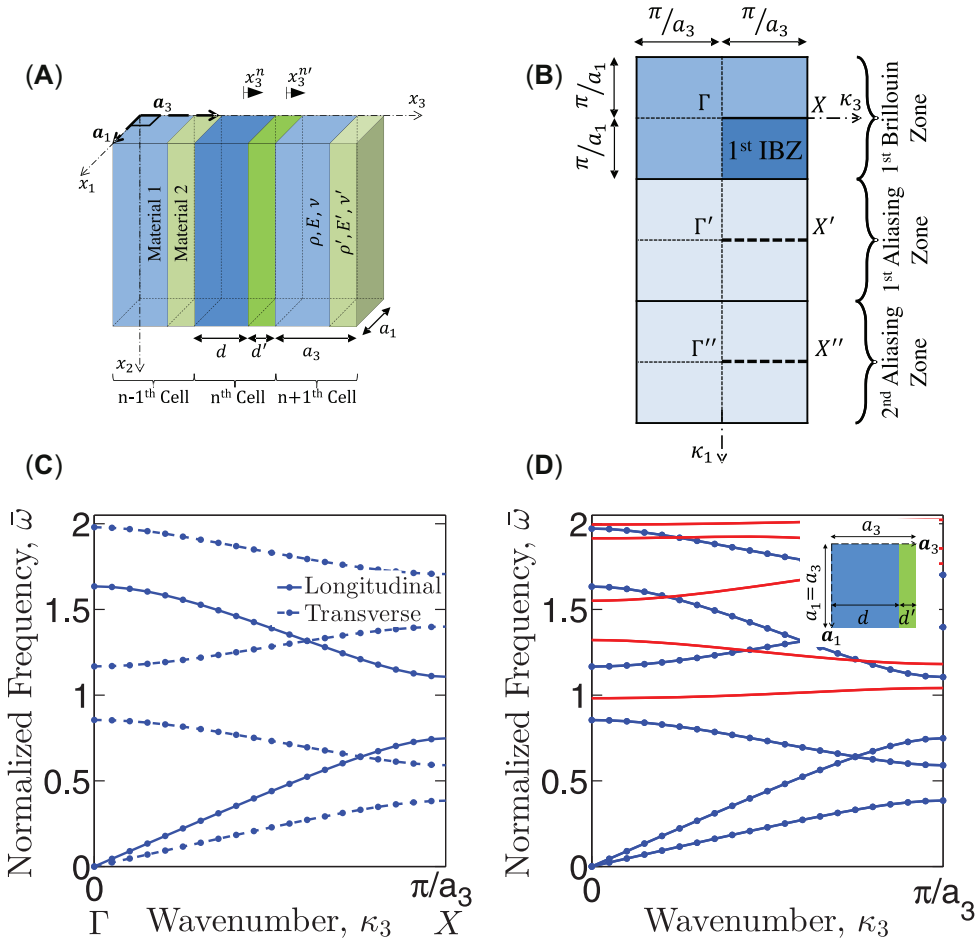

Fig. 1. (A) Geometry of a bi-material layered composite, which is infinitely periodic. The composite can be described by using a unit cell spanned by the primitive lattice vectors $\mathbf{a}_1$ and $\mathbf{a}_3$ in a 2-D coordinate space. Note that $a_1 = \|\mathbf{a}_1\|$ and $a_3 = \|\mathbf{a}_3\|$. (B) The corresponding wavevector space of the composite. The first Brillouin zone is the topmost rectangle delineated by a solid line, and aliasing zones are the results of spatial discretization in the x_1-axis. (C) Analytical dispersion relations of wave motion perpendicular to the layers based on (20). Note that the normalized frequency $\bar{\omega}$ is defined by $\bar{\omega} = \omega a_3/(2\pi c_s')$. (D) Numerical dispersion relations calculated in the conventional FE framework, where a unit cell having the aspect ratio of $a_1/a_3 = 1.0$ is used. Note that the numerical dispersion relations contain unwanted modes represented by red solid lines. (For interpretation of the references to colour in this figure legend, the reader is referred to the web version of this article.)

the sampling frequency is at least twice as large as the highest frequency contained within the continuous signal (or the highest frequency of interest). This principle is called the Nyquist theorem (Newland, 1993), and it determines a proper sampling time interval (Δt) for the highest frequency of interest (ω_{max}):

$$\Delta t < \frac{\pi}{\omega_{max}} \tag{1}$$

In this study, we investigate the occurrence of fictitious modes observed in the numerical dispersion relations of layered composites (i.e., 1-D phononic crystals) using the concept of spatial aliasing, which is analogous to temporal aliasing. Note that for waves parallel to the layers Mace and Manconi (2008); Manconi (2008) investigated spatial aliasing to study spectral distortions in the dispersion relations obtained from the WFE method. In the conventional FE framework, the phononic dispersion analysis of wave propagation perpendicular to the composite layers requires the use of a rectangular unit cell in a 2-D coordinate space. Although the properties of layered composites are continuous in the direction parallel to the layers (i.e., the x_1-axis in Fig. 1A), the 2-D modeling for a unit cell in the conventional FE procedure introduces spatial discretization in the x_1-axis, eventually causing fictitious modes in the corresponding wavevector domain (i.e. along the κ_1-axis). This study will demonstrate that the fictitious modes observed in numerical dispersion relations are the results of spatial aliasing in the wavevector domain.

This section contains cornerstones required to examine the origin of the numerical spectrum distortion in dispersion relations for wave motion perpendicular to the layers. The fundamentals of wave motion in phononic crystals are presented at first, and then they are followed by analytical dispersion solutions and numerical implementation procedure in the conventional FE framework.

2.1. Wave motion in 2-D phononic crystals

In this study, 2-D phononic crystals defined in the $x_1 - x_3$ plane (see Fig. 1A) are considered because a rectangular unit cell is employed in the numerical dispersion analysis of layered composites.

2.1.1. 2-D crystal lattice and the reciprocal lattice

For an infinitely periodic lattice spanning in the 2-D coordinate space, the corresponding Bravais lattice is described by a parallelogram with primitive lattice vectors $\mathbf{a}_1$ and $\mathbf{a}_3$. Any

spatially periodic function $\upsilon(\mathbf{x})$ is characterized by:

$$\upsilon(\mathbf{x}+\mathbf{r}) = \upsilon(\mathbf{x}) \tag{2}$$

where $\mathbf{x}$ denotes spatial position vectors in the $x_1 - x_3$ plane, and $\mathbf{r}$ is a set of the lattice vectors defined by:

$$\mathbf{r} = r_{a1}\mathbf{a}_1 + r_{a3}\mathbf{a}_3 \tag{3}$$

with arbitrary integers r_{a1} and r_{a3}. Here, the function $\upsilon(\mathbf{x})$ is called $\mathbf{r}$-periodic. One of the most commonly employed primitive unit cells is the Wigner–Seitz unit cell, which is defined by the region of space that is closer to a considered lattice point than any other lattice points (Ashcroft and Mermin, 1976).

The periodic function $\upsilon(\mathbf{x})$ can be expanded by using the complex Fourier series:

$$\upsilon(\mathbf{x}) = \sum_{\mathbf{g}} \hat{\upsilon}_{\mathbf{g}} e^{i\mathbf{g}\cdot\mathbf{x}} \tag{4}$$

where $\mathbf{g}$ denotes a set of the reciprocal lattice vectors, and $\hat{\upsilon}_{\mathbf{g}}$ represents the Fourier coefficients. In (4), the sum is over all reciprocal lattice vectors $\mathbf{g}$, which constitutes the reciprocal lattice of the given Bravais lattice. Here, the reciprocal lattice vectors $\mathbf{g}$ can be defined by:

$$\mathbf{g} = g_{b1}\mathbf{b}_1 + g_{b3}\mathbf{b}_3 \tag{5}$$

where g_{b1} and g_{b3} are arbitrary integers, and the primitive reciprocal lattice vectors $\mathbf{b}_1$ and $\mathbf{b}_3$ can be described by:

$$\mathbf{b}_1 = 2\pi \frac{\hat{\mathbf{e}}_2 \times \mathbf{a}_3}{\|\mathbf{a}_1 \times \mathbf{a}_3\|}, \quad \mathbf{b}_3 = 2\pi \frac{\mathbf{a}_1 \times \hat{\mathbf{e}}_2}{\|\mathbf{a}_1 \times \mathbf{a}_3\|} \tag{6}$$

with the Euclidean norm $\|\cdot\|$ and $\hat{\mathbf{e}}_2 = \frac{\mathbf{a}_3 \times \mathbf{a}_1}{\|\mathbf{a}_3 \times \mathbf{a}_1\|}$, so that $\mathbf{a}_p \cdot \mathbf{b}_q = 2\pi\delta_{pq}$ for $p, q = 1, 3$. Note that any wavevector $\boldsymbol{\kappa}$ in the reciprocal space (e.g., the $\kappa_1 - \kappa_3$ plane in Fig. 1B) can be written as a linear combination of $\mathbf{b}_1$ and $\mathbf{b}_3$. Moreover, the Fourier coefficients $\hat{\upsilon}_{\mathbf{g}}$ in (4) are given by:

$$\hat{\upsilon}_{\mathbf{g}} = \frac{1}{|\Omega|}\int_{\Omega} \upsilon(\mathbf{x}) e^{-i\mathbf{g}\cdot\mathbf{x}} d\Omega \tag{7}$$

where Ω represents any primitive unit cell and $|\Omega|$ denotes the area of the primitive unit cell. The Wigner–Seitz unit cell of the reciprocal lattice is called the first Brillouin zone. For the rectangular unit cell of layered composites, the first Brillouin zone is illustrated as the topmost rectangle delineated by a solid line in Fig. 1B. If the first Brillouin zone is invariant under certain rotational or mirror reflectional transformations, it can be further reduced by all of the symmetries in the point group of the reciprocal lattice. The reduced zone is referred as the first irreducible Brillouin zone (IBZ) (see Fig. 1B).

2.1.2. Discrete Fourier transform and spatial aliasing

Let $\chi(\mathbf{x})$ be an unknown continuous spatial function in the 2-D coordinate space. Assume that only regularly spaced $N_1 \times N_3$ data are available in a sampled region $x_1 \in \left(0, (N_1 - 1)\Delta x_1\right)$ and $x_3 \in \left(0, (N_3 - 1)\Delta x_3\right)$, and the discrete series $\{\chi[p_1, p_3]\}$ are denoted by $\chi[0, 0]$, $\chi[1, 0]$, ... , $\chi[N_1 - 1, N_3 - 1]$. In this case, the Fourier coefficients $\hat{\chi}_{\mathbf{g}}$ of the unknown continuous function $\chi(\mathbf{x})$ may be approximated by the summation (Bracewell, 2003):

$$\hat{\chi}_{\mathbf{g}} \approx \hat{\chi}[q_1, q_3] = \frac{1}{N_1 N_3}\sum_{p_1=0}^{N_1-1}\sum_{p_3=0}^{N_3-1} \chi[p_1, p_3] e^{-i2\pi\left(\frac{p_1 q_1}{N_1} + \frac{p_3 q_3}{N_3}\right)} \tag{8}$$

which is called the discrete Fourier transform (DFT) of the series $\{\chi[p_1, p_3]\}$. Since there are only a finite number of data points, the DFT treats the data as if they were periodic, resulting in the discrete values of $\hat{\chi}[q_1, q_3]$ over the $\kappa_1 - \kappa_3$ plane. Any typical value of $\chi[p_1, p_3]$ is exactly recovered from the series $\left\{\hat{\chi}[q_1, q_3]\right\}$ by the inverse formula:

$$\chi[p_1, p_3] = \sum_{q_1=0}^{N_1-1}\sum_{q_3=0}^{N_3-1} \hat{\chi}[q_1, q_3] e^{i2\pi\left(\frac{p_1 q_1}{N_1} + \frac{p_3 q_3}{N_3}\right)}. \tag{9}$$

The equally spaced discrete data $\chi[p_1, p_3]$ in the coordinate space engender the periodicity of the DFT coefficients:

$$\hat{\chi}[q_1, q_3] = \hat{\chi}[l_1 N_1 + q_1, l_3 N_3 + q_3] \tag{10}$$

where l_1 and l_3 are arbitrary integers. Furthermore, if $\chi(\mathbf{x})$ is a real-valued function, its DFT coefficients are conjugate symmetric with respect to the origin:

$$\hat{\chi}[q_1, q_3] = \hat{\chi}^*[-q_1, -q_3] \tag{11}$$

where $\square^*$ denote the complex conjugate. Therefore, the DFT coefficients $\hat{\chi}[q_1, q_3]$ are the only correct Fourier coefficients for the wavevector domain of $\kappa_1 \in (0, \pi/\Delta x_1)$ and $\kappa_3 \in (0, \pi/\Delta x_3)$, which coincides to the first Brillouin zone. In particular, due to the periodicity of the DFT in (10), there are infinitely many aliases of the true spectrum in the wavevector domain.

If the original continuous function $\chi(\mathbf{x})$ contains wavevector components beyond the wavevector domain of $\kappa_1 \in (0, \pi/\Delta x_1)$ and $\kappa_3 \in (0, \pi/\Delta x_3)$, the DFT coefficients will be corrupted and this numerical phenomenon is called spatial aliasing (Bracewell, 2003). The high wavevector components contribute to the $\chi[p_1, p_3]$ series, and falsely distort the DFT coefficients within in the wavevector domain of $\kappa_1 \in (0, \pi/\Delta x_1)$, $\kappa_3 \in (0, \pi/\Delta x_3)$. Since spatial aliasing occurs due to the discretization which are not sufficiently small to represent high-wavenumber components present in the continuous function, the solution is to increase the sampling rate.

Now, consider the rectangular unit cell of $a_1 \times a_3$ employed for the dispersion relations of a layered composite shown in Fig. 1A, where $a_1 = \|\mathbf{a}_1\|$ and $a_3 = \|\mathbf{a}_3\|$. The sampling with $\Delta x_3 = a_3$ in the direction perpendicular to the layers is small enough to capture the highest κ_3 component $\kappa_{3,f} = \pi/a_3$ of wave motion in the layered composite. However, due to the continuous properties of the layered composite in the direction parallel to the layers, the sampling with $\Delta x_1 = a_1$ is not sufficiently small to capture infinitely large κ_1 components. Eventually, this coarse spatial discretization in the x_1-axis induces the artificial $2\pi/a_1$-periodicity along the κ_1-axis of the wavevector domain and the calculated spectral behavior is distorted by the existence of the high-wavenumber components from an infinite number of aliasing zones of the first Brillouin zone (see Fig. 1B). For instance, the wavevector path denoted by $\Gamma - X$ has an infinite number of aliasing paths, i.e., $\Gamma' - X'$, $\Gamma'' - X''$, $\Gamma''' - X'''$, etc.

2.1.3. Bloch theorem

The Bloch theorem states that elastic wave motion with a wavevector $\boldsymbol{\kappa}$ (i.e., $\mathbf{u} = e^{i\boldsymbol{\kappa}\cdot\mathbf{x}}$) within a $\mathbf{r}$-periodic structure must satisfy the Bloch-periodic condition (Ashcroft and Mermin, 1976):

$$\mathbf{u}(\mathbf{x}+\mathbf{r}) = \mathbf{u}(\mathbf{x}) e^{i\boldsymbol{\kappa}\cdot\mathbf{r}}. \tag{12}$$

From the Bloch-periodic condition, the elastic wave motion within the $\mathbf{r}$-periodic structure is also found to be $\mathbf{g}$-periodic in the reciprocal lattice space (Ashcroft and Mermin, 1976):

$$\omega(\boldsymbol{\kappa}+\mathbf{g}) = \omega(\boldsymbol{\kappa}) \quad , \tag{13}$$

which indicates the $\mathbf{g}$-periodicity of the eigenvalue frequency ω of the considered periodic structure. Thus, only a subset of the wavevector domain is sufficient to be considered for obtaining the phononic dispersion relations of periodic structures, and it is a common practice to consider only wavevectors on the boundaries of the first IBZ (Maldovan and Thomas, 2009).

2.2. Analytic dispersion relations

Wave motion in 3-D elastic solids consists of two basic types of waves: P-wave (pressure wave) and S-wave (shear wave). Here, S-waves polarized in the horizontal and vertical planes are classified as SH-wave and SV-wave, respectively. The motion of P- and SV-waves are generally coupled, and the plane in which both waves propagate is referred as the sagittal plane. On the other hand, the motion of SH-wave is independent of the sagittal plane waves (Graff, 1991; Rouhani et al., 1983). For wave propagation perpendicular to the composite layers, the distinction between two shear waves disappears and P- and S-waves become uncoupled. Thus, in order to investigate wave motion in the plane including the direction perpendicular to the layers, it is sufficient to consider the sagittal plane waves. This subsection briefly reviews the analytical dispersion relations for waves in the sagittal plane as well as for waves perpendicular to the layers.

Consider an infinitely periodic layered composite, whose period in the x_3-axis is a_3 (see Fig. 1A). Each period consists of two isotropic elastic materials, Material 1 with thickness d and Material 2 with d' so that $a_3 = d + d'$. For Material 1, the mass density is denoted by ρ and the elastic properties are given by $c_{11} = \lambda + 2\mu$, $c_{44} = \mu$ and $c_{12} = c_{11} - 2c_{44} = \lambda$, where λ and μ are Lamé constants. Furthermore, its pressure and shear wave velocities are denoted by $c_p = \sqrt{c_{11}/\rho}$ and $c_s = \sqrt{c_{44}/\rho}$, respectively. Similarly, those of Material 2 are given by ρ', c'_{11}, c'_{44}, c'_{12}, λ', μ', c'_p and c'_s.

2.2.1. Waves propagation perpendicular to composite layers

Several references (He et al., 1988; Lee and Yang, 1973; Rytov, 1956) can be found for the detail derivation of the analytical dispersion relations for wave motion perpendicular to the layers, but here we provide only a brief summary of the transfer matrix method. Due to the complex nature of the equation of motion in layered composites, the displacement field $\mathbf{u}$ is resolved into the sum of the contribution from a dilatation-related scalar potential Φ and the contribution from a rotation-related vector potential $\mathbf{H}$ using Helmholtz's decomposition, $\mathbf{u} = \nabla\Phi + \nabla \times \mathbf{H}$ with $\nabla \cdot \mathbf{H} = 0$ (Graff, 1991). Now, the dispersion relations can be obtained by pursuing the conditions under which the plane waves represented by harmonic potentials may propagate in layered composites. By introducing local coordinates x_3^n and $x_3^{n'}$ in the n-th unit cell for Materials 1 and 2, respectively, the displacements of wave motion perpendicular to the layers can be represented by:

$$\begin{aligned} u_3^n(x_3^n, t) &= (P_R^n\ e^{i\omega x_3^n/c_p} + P_L^n\ e^{-i\omega x_3^n/c_p})\ e^{-i\omega t} \\ u_1^n(x_3^n, t) &= (Q_R^n\ e^{i\omega x_3^n/c_s} + Q_L^n\ e^{-i\omega x_3^n/c_s})\ e^{-i\omega t} \end{aligned} \tag{14}$$

for Material 1 and:

$$\begin{aligned} u_3^{n'}(x_3^{n'}, t) &= (P_R^{n'}\ e^{i\omega x_3^{n'}/c'_p} + P_L^{n'}\ e^{-i\omega x_3^{n'}/c'_p})\ e^{-i\omega t} \\ u_1^{n'}(x_3^{n'}, t) &= (Q_R^{n'}\ e^{i\omega x_3^{n'}/c'_s} + Q_L^{n'}\ e^{-i\omega x_3^{n'}/c'_s})\ e^{-i\omega t} \end{aligned} \tag{15}$$

for Material 2. Here, P_R^n, P_L^n, Q_R^n, Q_R^n, $P_R^{n'}$, $P_L^{n'}$, $Q_R^{n'}$, $Q_R^{n'}$ are the unknown constants to be determined from the continuous boundary conditions of the displacements and stresses at interfaces. Applying the Bloch-periodic condition (12), one can simultaneously obtain two decoupled eigenvalue problems for pressure and shear waves.

As an illustration, the application of the continuous boundary conditions for pressure wave motion gives (He et al., 1988):

$$\mathbf{T}_1\mathbf{W}_n = \mathbf{W}_{n+1} \tag{16}$$

where

$$\mathbf{W}_n = \begin{bmatrix} P_R^n \\ P_L^n \end{bmatrix} \quad , \quad \mathbf{W}_{n+1} = \begin{bmatrix} P_R^{n+1} \\ P_L^{n+1} \end{bmatrix} \quad , \tag{17}$$

$$\mathbf{T}_1 = \begin{bmatrix} e^{\frac{i\omega d}{c_p}}\left[\cos\left(\frac{\omega d'}{c'_p}\right) + \frac{i}{2}\left(\frac{\rho c_p}{\rho' c'_p} + \frac{\rho' c'_p}{\rho c_p}\right)\sin\left(\frac{\omega d'}{c'_p}\right)\right] & e^{\frac{-i\omega d}{c_p}}\left[\frac{i}{2}\left(\frac{\rho c_p}{\rho' c'_p} - \frac{\rho' c'_p}{\rho c_p}\right)\sin\left(\frac{\omega d'}{c'_p}\right)\right] \\ e^{\frac{i\omega d}{c_p}}\left[\frac{i}{2}\left(\frac{\rho c_p}{\rho' c'_p} - \frac{\rho' c'_p}{\rho c_p}\right)\sin\left(\frac{\omega d'}{c'_p}\right)\right] & e^{\frac{-i\omega d}{c_p}}\left[\cos\left(\frac{\omega d'}{c'_p}\right) - \frac{i}{2}\left(\frac{\rho c_p}{\rho' c'_p} + \frac{\rho' c'_p}{\rho c_p}\right)\sin\left(\frac{\omega d'}{c'_p}\right)\right] \end{bmatrix} \tag{18}$$

Here, $\mathbf{T}_1$ is the transfer matrix for pressure wave motion perpendicular to the layers. By applying the Bloch-periodic boundary condition between adjacent unit cells (12):

$$\mathbf{W}_{n+1} = e^{i\kappa_3 a_3}\mathbf{W}_n \quad , \tag{19}$$

one can obtain an eigenvalue problem for the pressure wave motion:

$$\mathbf{T}_1\mathbf{W}_n = e^{i\kappa_3 a_3}\mathbf{W}_n \tag{20}$$

where $e^{i\kappa_3 a_3}$ and $\mathbf{W}_n$ are the eigenvalue and the eigenvector of $\mathbf{T}_1$, respectively. By solving this eigenvalue problem, the dispersion relations for pressure wave propagation perpendicular to the layers is analytically obtained:

$$\begin{aligned} \cos(a_3\kappa_3) = &\cos\left(\frac{\omega d}{c_p}\right)\cos\left(\frac{\omega d'}{c'_p}\right) \\ &- \frac{1}{2}\left(\frac{\rho c_p}{\rho' c'_p} + \frac{\rho' c'_p}{\rho c_p}\right)\sin\left(\frac{\omega d}{c_p}\right)\sin\left(\frac{\omega d'}{c'_p}\right) \quad . \end{aligned} \tag{21}$$

Moreover, a similar expression for shear wave propagation perpendicular to the layers can be obtained:

$$\begin{aligned} \cos(a_3\kappa_3) = &\cos\left(\frac{\omega d}{c_s}\right)\cos\left(\frac{\omega d'}{c'_s}\right) \\ &- \frac{1}{2}\left(\frac{\rho c_s}{\rho' c'_s} + \frac{\rho' c'_s}{\rho c_s}\right)\sin\left(\frac{\omega d}{c_s}\right)\sin\left(\frac{\omega d'}{c'_s}\right) \quad . \end{aligned} \tag{22}$$

Both (21) and (22) constitute the closed form solution of the phononic dispersion relations for wave motion perpendicular to the composite layers.

2.2.2. Waves propagation at arbitrary angle in the sagittal plane

This subsection briefly revisits the analytical dispersion relations of layered composites for the sagittal plane waves, which can be found in several references (Nougaoui and Rouhani, 1987; Rouhani et al., 1983; Sapriel and Rouhani, 1989). As mentioned in Section 2.2.1, the first step is to apply Helmholtz's decomposition to obtain a representative form for the displacement field $\mathbf{u}$. Unlike wave motion perpendicular to the layers, the displacement field in the sagittal plane (i.e., the $x_3 - x_1$ plane) is now a function of x_1, x_3 and t. Thus, the dispersion relations in the sagittal plane should be determined in the $\kappa_3 - \kappa_1$ wavevector space, resulting in a 3-D plot (i.e., ω over the $\kappa_3 - \kappa_1$ plane). Considering the symmetry of layered composites, the valid range for the κ_1-axis is $(0, \infty)$ while κ_3 should range over $(0, \pi/a_3)$ which is the true first IBZ.

Instead of pursuing a numerical solution for the phononic dispersion relations in the sagittal plane, Rouhani et al. (1983) presented a semi-analytical approach by solving the governing equations with boundary conditions at a given κ_1. By sweeping κ_1, the complete picture of the dispersion relations can be obtained. So,

for a given κ_1 value, the n-th unit cell displacement in the sagittal plane (i.e., $x_3 - x_1$ plane) can be expressed by:

$$\begin{aligned} u_1(x_3^n,t) &= [A_L^n\cosh(\alpha_L x_3^n) + A_T^n\cosh(\alpha_T x_3^n) - B_L^n\sinh(\alpha_L x_3^n) \\ &\quad - B_T^n\sinh(\alpha_T x_3^n)]e^{i(\kappa_1 x_1-\omega t)} \\ u_3(x_3^n,t) &= i\Big[-\frac{\alpha_L}{\kappa_1}A_L^n\sinh(\alpha_L x_3^n) - \frac{\kappa_1}{\alpha_T}A_T^n\sinh(\alpha_T x_3^n) \\ &\quad + \frac{\alpha_L}{\kappa_1}B_L^n\cosh(\alpha_L x_3^n) + \frac{\kappa_1}{\alpha_T}B_T^n\cosh(\alpha_T x_3^n)\Big]e^{i(\kappa_1 x_1-\omega t)} \end{aligned} \tag{23}$$

for Material 1 and:

$$\begin{aligned} u_1'(x_3^{n'},t) &= [A_L^{n'}\cosh(\alpha_L' x_3^{n'}) + A_T^{n'}\cosh(\alpha_T' x_3^{n'}) \\ &\quad - B_L^{n'}\sinh(\alpha_L' x_3^{n'}) - B_T^{n'}\sinh(\alpha_T' x_3^{n'})]e^{i(\kappa_1 x_1-\omega t)} \\ u_3'(x_3^{n'},t) &= i\Big[-\frac{\alpha_L'}{\kappa_1}A_L^{n'}\sinh(\alpha_L' x_3^{n'}) - \frac{\kappa_1}{\alpha_T'}A_T^{n'}\sinh(\alpha_T' x_3^{n'}) \\ &\quad + \frac{\alpha_L'}{\kappa_1}B_L^{n'}\cosh(\alpha_L' x_3^{n'}) + \frac{\kappa_1}{\alpha_T'}B_T^{n'}\cosh(\alpha_T' x_3^{n'})\Big]e^{i(\kappa_1 x_1-\omega t)} \end{aligned} \tag{24}$$

for Material 2. Here, $\alpha_L = \sqrt{(\kappa_1^2 - \omega^2/c_p^2)}$, $\alpha_T = \sqrt{(\kappa_1^2 - \omega^2/c_s^2)}$ are determined through the governing equations of motion, and α_L' and α_T' are also similarly defined using the properties of Material 2. Furthermore, unknown coefficients A_L^n, A_T^n, B_L^n, B_T^n, $A_L^{n'}$, $A_T^{n'}$, $B_L^{n'}$ and $B_T^{n'}$ can be determined by employing the continuous displacement and stress boundary conditions at interfaces.

After applying the continuous boundary conditions for the displacements and stresses at interfaces (Rouhani et al., 1983), one can obtain a relations where pressure and shear waves are coupled:

$$\mathbf{T}_2\mathbf{V}_n = \mathbf{V}_{n+1} \tag{25}$$

where

$$\mathbf{T}_2 = \mathbf{Q}^{-1}\mathbf{P}'\mathbf{Q}'^{-1}\mathbf{P} \quad , \tag{26}$$

$$\mathbf{V}_n = \begin{bmatrix} A_L^n \\ A_T^n \\ B_L^n \\ B_T^n \end{bmatrix} \quad , \quad \mathbf{V}_{n+1} = \begin{bmatrix} A_L^{n+1} \\ A_T^{n+1} \\ B_L^{n+1} \\ B_T^{n+1} \end{bmatrix} \quad , \tag{27}$$

$$\mathbf{P} = \begin{bmatrix} C_L & C_T & -S_L & -S_T \\ -\alpha_L S_L & -\frac{\kappa_1^2}{\alpha_T}S_T & \alpha_L C_L & \frac{\kappa_1^2}{\alpha_T}C_T \\ 2\alpha_L c_{44} S_L & c_{44}\left(\alpha_T + \frac{\kappa_1^2}{\alpha_T}\right)S_T & -2\alpha_L c_{44} C_L & -c_{44}\left(\alpha_T + \frac{\kappa_1^2}{\alpha_T}\right)C_T \\ \left(c_{12}\kappa_1^2 - c_{11}\alpha_L^2\right)C_L & (c_{12}-c_{11})\kappa_1^2 C_T & -\left(c_{12}\kappa_1^2 - c_{11}\alpha_L^2\right)S_L & -(c_{12}-c_{11})\kappa_1^2 S_T \end{bmatrix}, \tag{28}$$

$$\mathbf{Q} = \begin{bmatrix} C_L & C_T & S_L & S_T \\ \alpha_L S_L & \frac{\kappa_1^2}{\alpha_T}S_T & \alpha_L C_L & \frac{\kappa_1^2}{\alpha_T}C_T \\ -2\alpha_L c_{44} S_L & -c_{44}\left(\alpha_T + \frac{\kappa_1^2}{\alpha_T}\right)S_T & -2\alpha_L c_{44} C_L & -c_{44}\left(\alpha_T + \frac{\kappa_1^2}{\alpha_T}\right)C_T \\ \left(c_{12}\kappa_1^2 - c_{11}\alpha_L^2\right)C_L & (c_{12}-c_{11})\kappa_1^2 C_T & \left(c_{12}\kappa_1^2 - c_{11}\alpha_L^2\right)S_L & (c_{12}-c_{11})\kappa_1^2 S_T \end{bmatrix}, \tag{29}$$

with $C_L = \cos(\alpha_L d/2)$, $C_T = \cos(\alpha_T d/2)$, $S_L = \sin(\alpha_L d/2)$ and $S_T = \sin(\alpha_T d/2)$. Similarly, $\mathbf{P}'$, $\mathbf{Q}'$, C_L', C_T', S_L', and S_T' are defined using the properties of Material 2. Here, the transfer matrix $\mathbf{T}_2$ determines the relation between the coefficient vectors ($\mathbf{V}_n$ and $\mathbf{V}_{n+1}$) of adjacent unit cells in the sagittal plane. Furthermore, the Bloch-periodic condition (12) also relates wave motion between adjacent unit cells:

$$\mathbf{V}_{n+1} = e^{i\kappa_3 a_3}\mathbf{V}_n. \tag{30}$$

Eventually, combining (25) and (30), one can obtain the eigenvalue problem of wave motion in the sagittal plane for a given κ_1:

$$\mathbf{T}_2\mathbf{V}_n = e^{i\kappa_3 a_3}\mathbf{V}_n. \tag{31}$$

For a fixed value of κ_1, this eigenvalue problem can be numerically solved for κ_3 and ω using (A.6). By sweeping κ_1 within the range of $(0, \infty)$, the complete picture of dispersion relations for the sagittal plane waves can be determined over the $\kappa_3 - \kappa_1$ plane. Note that the analytical dispersion relations (21) and (22) can also be obtained by solving (31) with $\kappa_1 = 0$, and its procedure is briefly given in the Appendix.

2.3. Numerical dispersion relations in the conventional FE framework

To calculate the dispersion relations $\omega = \omega(\boldsymbol{\kappa})$ within the conventional FE framework, the Bloch-periodic conditions (12) should be applied to the boundaries of the considered unit cell model. In order to work with the complex-valued relations of the Bloch-periodic conditions in a commercial FE software ABAQUS/Standard, all fields of the considered FE model are split into real and imaginary parts. In this way, the equilibrium equations are divided into two sets of uncoupled equations for the real and imaginary parts (Aberg and Gudmundson, 1997; Shim et al., 2015). In practice, two identical FE meshes for the unit cell (i.e., one for the real part and the other for the imaginary part) are coupled through the decomposed Bloch-periodic displacement boundary conditions:

$$\begin{aligned} \mathbf{u}_\beta^{re} &= \mathbf{u}_\alpha^{re}\cos(\boldsymbol{\kappa}\cdot\mathbf{r}_{\alpha\beta}) - \mathbf{u}_\alpha^{im}\sin(\boldsymbol{\kappa}\cdot\mathbf{r}_{\alpha\beta}) \\ \mathbf{u}_\beta^{im} &= \mathbf{u}_\alpha^{re}\sin(\boldsymbol{\kappa}\cdot\mathbf{r}_{\alpha\beta}) + \mathbf{u}_\alpha^{im}\cos(\boldsymbol{\kappa}\cdot\mathbf{r}_{\alpha\beta}) \end{aligned} \tag{32}$$

where the subscripts α and β are two nodal points periodically located on the boundaries of the unit cell, and the superscripts *re* and *im* denote the real and the imaginary part of the displacement field, respectively. In addition, $\mathbf{r}_{\alpha\beta} = \mathbf{x}_\beta - \mathbf{x}_\alpha$ represents the

distance between two nodal points denoted by α and β. Note that (32) is implemented in ABAQUS/Standard using a user defined subroutine MPC [ABAQUS]. For a given $\boldsymbol{\kappa}$ within the considered range of the wavevector domain, the corresponding frequencies ω are calculated by performing an eigenfrequency analysis in ABAQUS/Standard. The eigenfrequencies associated with each wavevector are then plotted in the dispersion diagram.

3. Results

This section describes the details of the materials and geometries for the considered layered composite, and reports its numerical and analytical dispersion relations.

3.1. Material and geometry

In order to investigate the origin of the spectral distortion observed in numerical dispersion relations, we choose a layered composite consisting of alternating layers of steel ($d = 0.8\ mm$) and aluminum ($d' = 0.2\ mm$). Thus, the period of the composite layers in the x_3-axis is $a_3 = d + d' = 1\ mm$. Steel is assumed to have the mass density of $\rho = 7800\ kg/m^3$, and the isotropic elastic properties of $\lambda = 121.2\ GPa$ and $\mu = 80.8\ GPa$. In addition, aluminum is assumed to have $\rho' = 2700\ kg/m^3$, $\lambda' = 51.1\ GPa$ and $\mu' = 26.3\ GPa$.

The emergence of the fictitious modes is investigated by varying the aspect ratio of a_1/a_3 in the considered unit cell, where a_1 is the length of the unit cell in the x_1-axis. For the given $a_3 = 1\ mm$, this study considers three different unit cell configurations: $a_1/a_3 = 2.0$, $a_1/a_3 = 1.0$ and $a_1/a_3 = 0.5$. Their geometries and corresponding Brillouin/aliasing zones are shown in Figs. 2A, 3A and 4A. In all the FE analyses, plane strain conditions are assumed and the 2-D models are constructed using 4-node bilinear plane strain elements (CPE4R elements in ABAQUS). A series of mesh refinement studies is preformed to assure the independency of numerically obtained dispersion relations on mesh sizes, and the mesh size of $0.025a_3$ is determined to ensure the convergence of the FE simulations.

3.2. Numerical dispersion relations

To clearly demonstrate the effect of the aspect ratio a_1/a_3 on the appearance of fictitious modes, the same vertical axis limit (i.e., frequency limit) of $\bar{\omega} = 2.1$ is employed in Figs. 2–4. Firstly, for the unit cell having the aspect ratio of $a_1/a_3 = 2.0$, Fig. 2B presents the results of the numerical dispersion analysis performed in the conventional FE framework, whose procedure is briefly described in Section 2.3. In this figure, the lines with dots are the desired dispersion relations for waves perpendicular to the layers, but in the conventional FE framework they cannot be separated from unwanted (i.e., fictitious) modes denoted by solid lines. Note that the modes denoted by the lines with dots are identified after comparing the FE solutions with the analytical solutions from (21) and (22). It is observed that fictitious modes from the FE analysis appear around the normalized frequency of $\bar{\omega} = \omega a_3/(2\pi c_s') = 0.5$.

Similarly, the numerical results of dispersion analysis with the unit cells of $a_1/a_3 = 1.0$ and 0.5 are described in Figs. 3B and 4B, respectively. Fictitious modes from the FE analysis with $a_1/a_3 = 1.0$ appear above $\bar{\omega} = 1.0$ (see Fig. 3B), and ones with $a_1/a_3 = 0.5$ emerge around $\bar{\omega} = 2.0$ (see Fig. 4B). For the case of $a_1/a_3 = 0.5$, note that fictions modes along $\Gamma'' - X''$ appear around $\bar{\omega} = 4.0$, which reside outside of the vertical axis limit of $\bar{\omega} = 2.1$. Hence, Fig. 4 does not include the dispersion relations along $\Gamma'' - X''$, which will be an empty graph having the limit of $\bar{\omega} = 2.1$. These numerical results illustrate again that special care should be taken in interpreting the FE results of dispersion analysis for waves perpendicular to the layers. In addition, it is clear that fictitious modes start to appear at higher frequencies as the aspect ratio a_1/a_3 decreases. This is why many researchers have been employing a thin unit cell, which is just a phenomenologically driven guideline (Aberg and Gudmundson, 1997; Minagawa and Nemat-Nasser, 1977; Minagawa et al., 1981).

3.3. Spatial aliasing and analytical dispersion relations

The spatial discretization by using a rectangular unit cell of $a_1 \times a_3$ entails the artificial $2\pi/a_1$-periodicity in the κ_1-axis of the wavevector domain. The aliases of the true phononic dispersion relations appear due to the $2\pi/a_1$-periodicity, and the spectrum are now symmetrical around a multiple of π/a_1 in the κ_1-axis. This symmetry is commonly referred as zone folding (Brillouin, 1946), and the folding wavenumber $\kappa_{1,f}$ is defined as:

$$\kappa_{1,f} = \frac{\pi}{a_1}. \tag{33}$$

However, wave motion in layered composites contains infinitely large κ_1 components. This fact can be verified by the analytical solution of the sagittal plane waves (described in Section 2.2.2), which enables us to identify the dispersion relations of layered composites at a specific wavevector path. Figs. 5A and 5B illustrate the analytical dispersion relations in the direction parallel to the layers by setting $\kappa_3 = 0$ and π/a_3, respectively. From these figures, it is clear that the numerically unreachable dispersion relations for $\kappa_1 \geq \kappa_{1,f}$ contribute to the true spectral behavior in the first Brillouin zone, and distort the dispersion relations of layered composites. In other words, the FE analysis results shown in Figs. 2B, 3B and 4B are composed of the true dispersion relations along $\Gamma - X$ (i.e., first Brillouin zone) and the contributions from aliases along $\Gamma' - X'$ (i.e., first aliasing zone), $\Gamma'' - X''$ (i.e., second aliasing zone), etc.

By exploring κ_1 values in the sagittal plane wave solution, one can calculate the contribution from the aliases due to the discretization in the x_1-axis. Firstly, Fig. 2C presents the sagittal plane wave solutions in order to compare them with the FE results using the unit cell having $a_1/a_3 = 2.0$. The three subfigures in Fig. 2C show the analytical results at three different κ_1 values (i.e., $\kappa_1 = 0$, $2\kappa_{1,f}$ and $4\kappa_{1,f}$), which correspond to a multiple of $2\kappa_{1,f}$. In a specific way, Fig. 2C-1 is obtained by solving (31) with $\kappa_1 = 0$, which corresponds to the path defined by $\Gamma - X$ shown in Fig. 2A. Note that the analytical results shown in Fig. 2C-1 are the dispersion relations that the conventional FE method fails to provide. Subsequently, the sagittal wave solutions of (31) at $\kappa_1 = 2\kappa_{1,f}$ (i.e., $\Gamma' - X'$) and $4\kappa_{1,f}$ (i.e., $\Gamma'' - X''$) are presented in Figs. 2C-2 and 2C-3, respectively.

Now, Fig. 2D shows the projection of all the analytical dispersion relations calculated at $\kappa_1 = 0$, $2\kappa_{1,f}$, $4\kappa_{1,f}$, $6\kappa_{1,f}$, etc. onto the $\kappa_3 - \omega$ plane of the dispersion relations diagram. For each mode in Fig. 2B which are calculated in the conventional FE framework, one can identify the corresponding semi-analytical sagittal plane wave mode shown in Fig. 2D. Thus, by observing the identical results from Figs. 2B and 2D, we indeed find that the fictitious modes in the dispersion relations are the contribution from the aliasing paths (i.e., $\Gamma' - X'$, $\Gamma'' - X''$, etc.) of the first Brillouin zone path (i.e., $\Gamma - X$).

In the same way, the analytical dispersion analysis with the unit cell having the aspect ratios of $a_1/a_3 = 1.0$ and 0.5 are also summarized in Figs. 3C/D and 4C/D, respectively. Again, we find that the fictitious numerical modes calculated in the conventional FE framework are the contribution from the aliasing path of the first Brillouin zone path $\Gamma - X$. In summary, using the analytical solution for the sagittal plane waves, we demonstrate that the fictitious

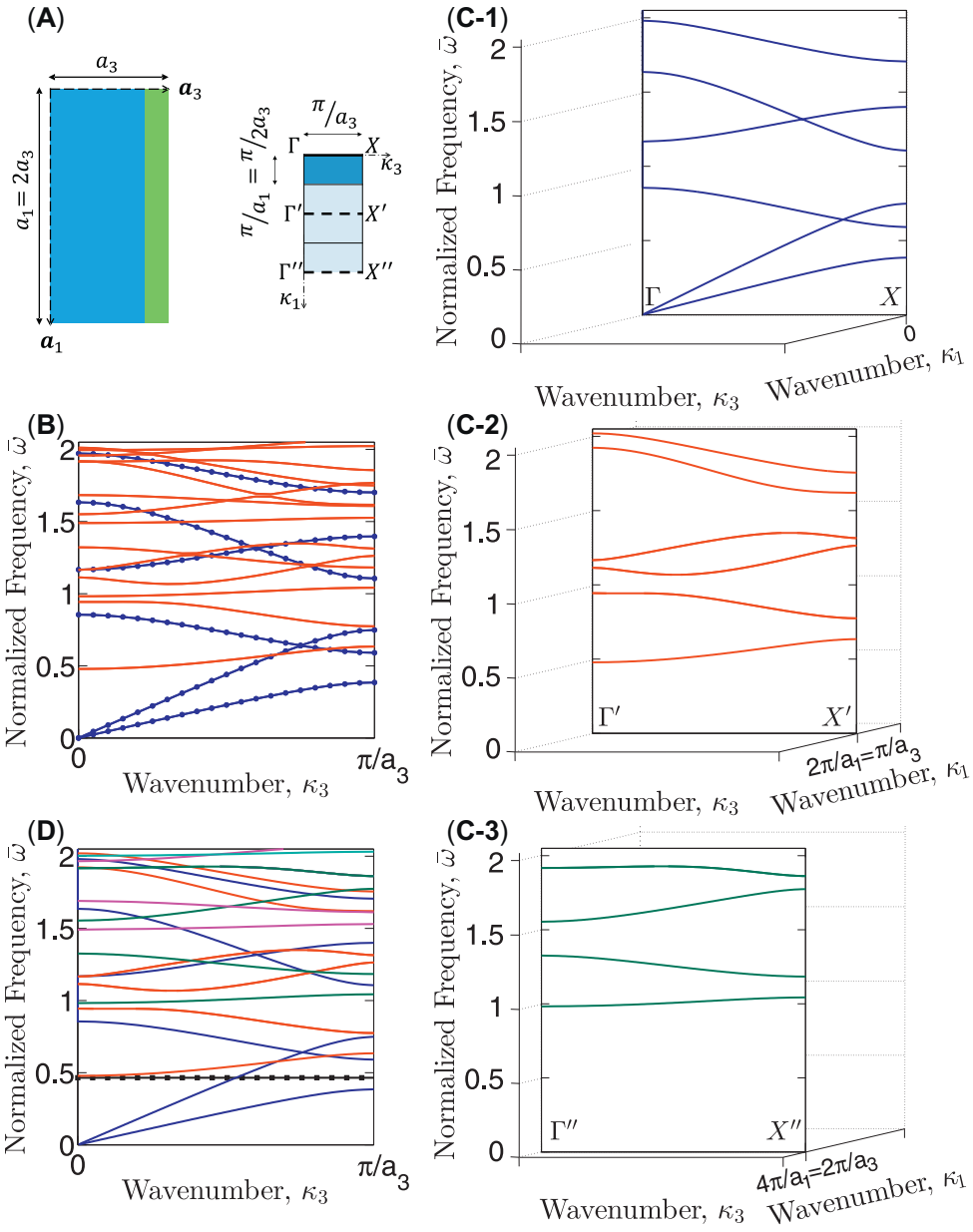

Fig. 2. (A) Left: unit cell having $a_1/a_3 = 2.0$, which is employed for numerical dispersion relations. Right: the corresponding wavevector domain, which illustrates the first Brillouin zone path ($\Gamma - X$) and the aliasing paths ($\Gamma' - X'$, $\Gamma'' - X''$). (B) FE dispersion relations obtained by employing the unit cell of $a_1/a_3 = 2.0$. Note that the numerical dispersion relations contain unwanted modes represented by red solid lines. (C) Three analytical dispersion relations obtained from (31) with $\kappa_1 = 0$ (C-1), $\kappa_1 = 2\pi/a_1$ (C-2), and $\kappa_1 = 4\pi/a_1$ (C-3). (D) The projection of all the analytical dispersion relations in Fig. 2C onto the $\kappa_3 - \omega$ plane. Note that one can find one-to-one map between the modes in Figs. 2B and 2D, indicating that the unwanted modes originate from the aliasing zones. Moreover, the maximum valid frequency $\omega_{1,\max}$ from (38) is denoted by a line with squares.

modes observed in the numerical dispersion relations (i.e., 2B, 3B and 4B) are the manifest results of spatial aliasing in the wavevector domain.

4. Discussion

In order to improve the numerical prediction of wave motion in various types of layered medium, many efforts have been made in the computational mechanics community. The WFE method (Duhamel et al., 2006; Houillon et al., 2005; Mace and Manconi, 2008; Manconi, 2008; Mencik and Ichchou, 2007; Waki et al., 2009) and the semi-analytical finite element (SAFE) method (Bartoli et al., 2006; Gavrić, 1994; Hladky-Hennion, 1996; Lagasse, 1973; Mukdadi and Datta, 2003) are developed to exactly represent wave motion along the direction parallel to the layers. Furthermore, both numerical techniques can be extended to obtain the dispersion relations of waves perpendicular to the layers without fictitious modes. In particular, Manconi (Manconi, 2008) extensively investigated the various aspects of spectral distortions in the dispersion relations obtained from the WFE method. The distortions induced by spatial aliasing found to originate from various sources such as the mesh dimensions, the direction of wave propagation and the aspect ratio of the unit cell. Through an extensive study with a wide range of mesh sizes and aspect ratios, all the fictitious modes were identified and the sensitivity of fictitious modes to model discretization was also analyzed in the WFE method.

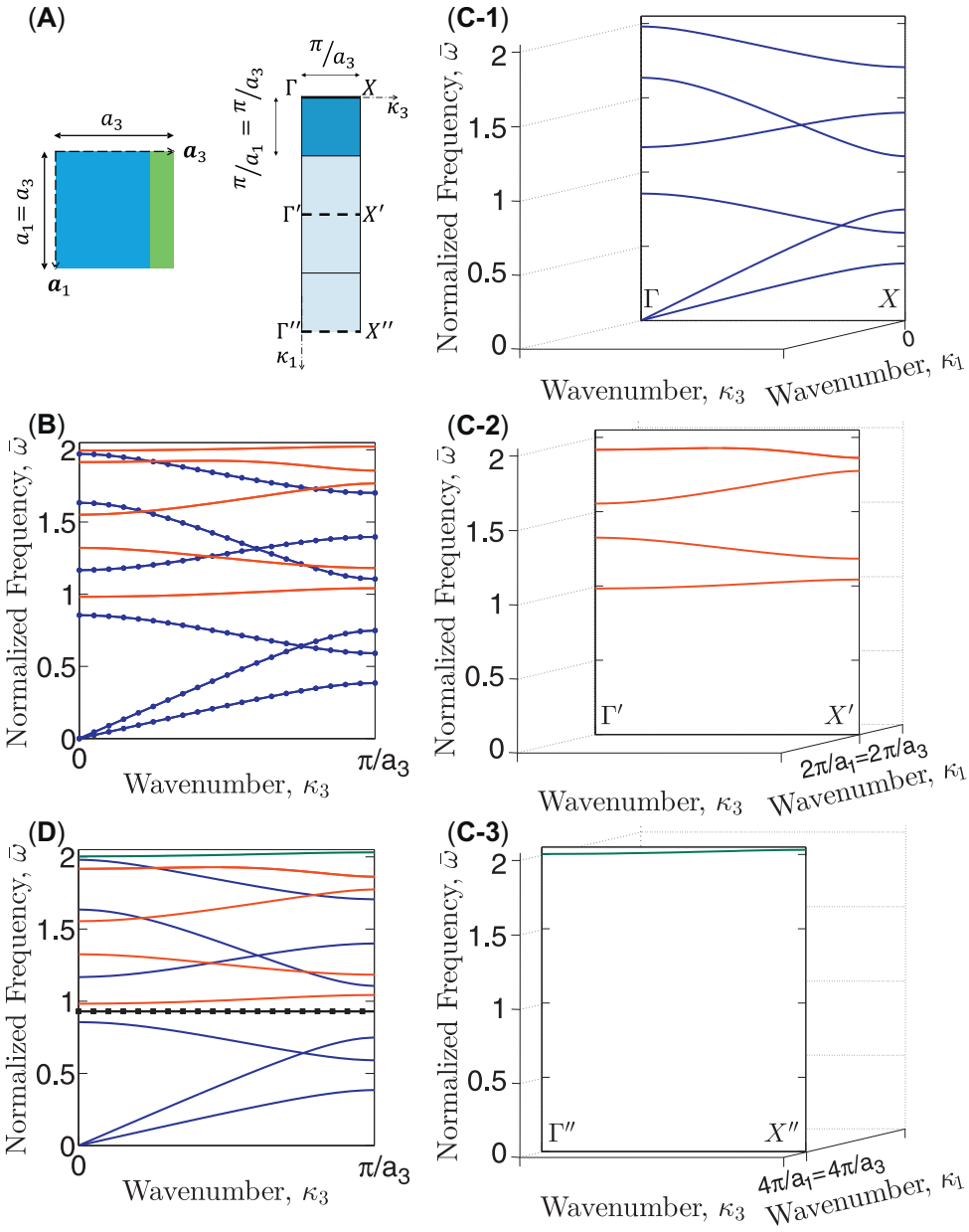

Fig. 3. (A) Left: unit cell having $a_1/a_3 = 1.0$, which is employed for numerical dispersion relations. Right: the corresponding wavevector domain, which illustrates the first Brillouin zone path ($\Gamma - X$) and the aliasing paths ($\Gamma' - X'$, $\Gamma'' - X''$). (B) FE dispersion relations obtained by employing the unit cell of $a_1/a_3 = 1.0$. Note that the numerical dispersion relations contain unwanted modes represented by red solid lines. (C) Three analytical dispersion relations obtained from (31) with $\kappa_1 = 0$ (C-1), $\kappa_1 = 2\pi/a_1$ (C-2), and $\kappa_1 = 4\pi/a_1$ (C-3). (D) The projection of all the analytical dispersion relations in Fig. 3C onto the $\kappa_3 - \omega$ plane. Note that one can find one-to-one map between the modes in Figs. 3B and 3D, indicating that the unwanted modes originate from the aliasing zones. Moreover, the maximum valid frequency $\omega_{1,\max}$ from (38) is denoted by a line with squares.

In this section, recalling the origin of spectral distortions in the dispersion relations obtained from the conventional FE method, we expect that researchers using the conventional FE method for dispersion analysis are alerted to the potential spectral distortions in the numerical results. The dispersion relations of layered composites for waves perpendicular to the layers can be obtained from the sagittal plane wave solution along the path defined by $\kappa_1 = 0$ and $\kappa_3 \in (0, \pi/a_3)$ (i.e., the wavevector path $\Gamma - X$ in Figs. 1B). Section 3.3 reveals that spatial discretization with $\Delta x_1 = a_1$ induces the symmetry along the folding wavenumber $\kappa_{1,f}$, beyond which the numerical dispersion relations cannot be obtained. Consequently, spectral distortion induced by spatial aliasing occurs at an infinite number of the aliasing paths which are located at a multiple of $2\kappa_{1,f}$ in the κ_1-axis, i.e., $\kappa_1 = 2\kappa_{1,f}$, $4\kappa_{1,f}$, $6\kappa_{1,f}$, etc. This idea leads to an anti-aliasing condition: numerical dispersion relations for waves perpendicular to the layers is valid before the first appearance of the fictitious modes:

$$\kappa_{1,max} < 2\kappa_{1,f} = \frac{2\pi}{a_1} \tag{34}$$

where $\kappa_{1,\max}$ is the maximum wavenumber that the numerical dispersion relations can be valid up to. It is worthwhile to mention that the anti-aliasing condition (29) is rather different from Petersen-Middleton theorem (Petersen and Middleton, 1962), which is a generalization of the Nyquist theorem in the wavevector domain (1). In order to prevent spatial aliasing over a certain wavevector range of interest (say, $\kappa_1 \in (0, \kappa_{1,f})$), the Petersen–Middleton theorem provides a proper sampling spatial interval ($\Delta x_1 = a_1 < \pi/\kappa_{1,f}$). However, for the case of the dispersion

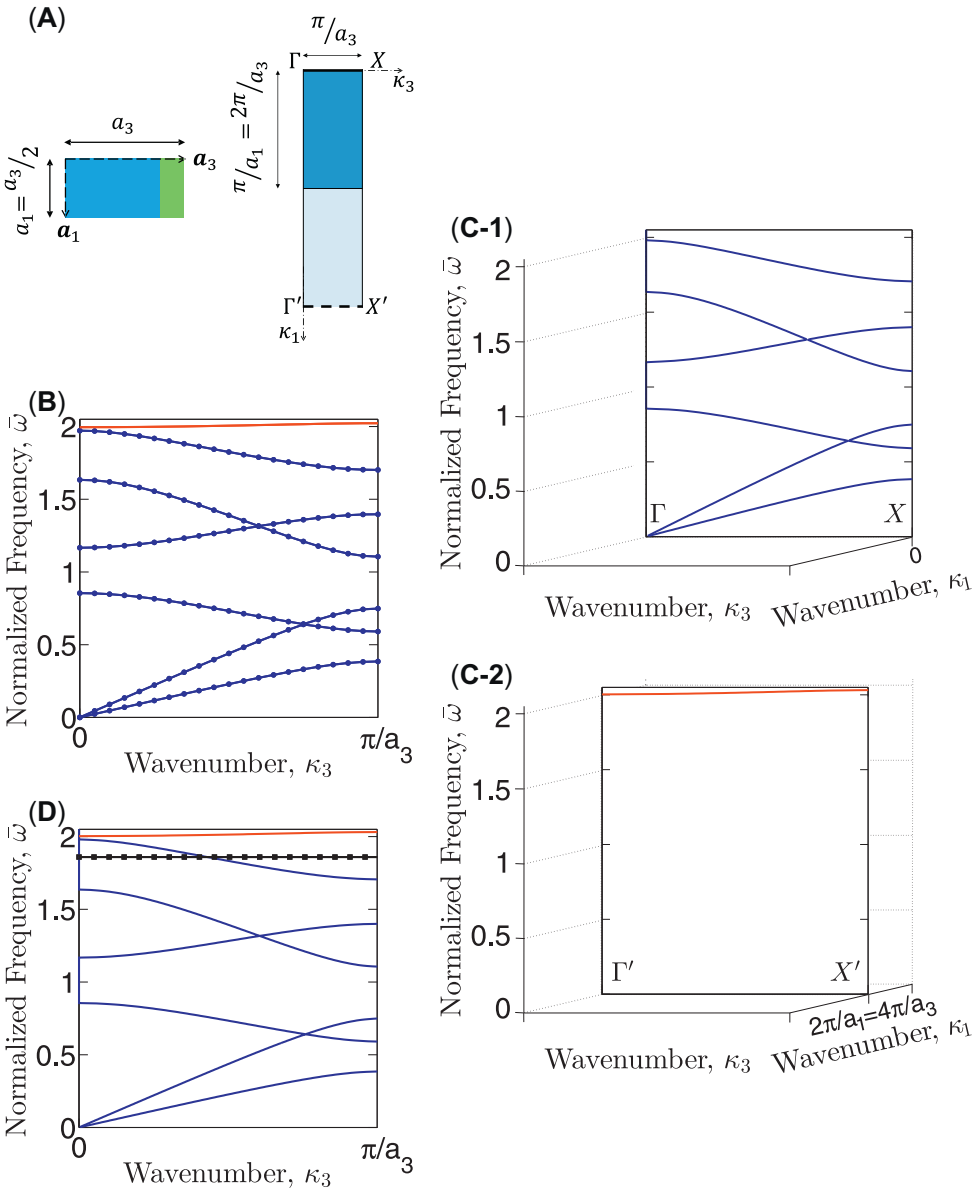

Fig. 4. (A) Left: unit cell having $a_1/a_3 = 0.5$, which is employed for numerical dispersion relations. Right: the corresponding wavevector domain, which illustrates the first Brillouin zone path ($\Gamma - X$) and the aliasing path ($\Gamma' - X'$). (B) FE dispersion relations obtained by employing the unit cell of $a_1/a_3 = 0.5$. Note that the numerical dispersion relations contain unwanted modes represented by red solid lines. (C) Three analytical dispersion relations obtained from (31) with $\kappa_1 = 0$ (C-1) and $\kappa_1 = 2\pi/a_1$ (C-2). (D) The projection of all the analytical dispersion relations in Fig. 4C onto the $\kappa_3 - \omega$ plane. Note that one can find one-to-one map between the modes in Fig. 4B and Fig. 4D, indicating that the unwanted modes originate from the aliasing zones. Moreover, the maximum valid frequency $\omega_{1,\max}$ from (38) is denoted by a line with squares.

relations of layered composites, the anti-aliasing condition (34) prevents only the spatial aliasing of the true spectrum at $\kappa_1 = 0$.

Practically, the anti-aliasing condition (34) can be used to determine a proper unit cell size a_1 prior to FE analyses, if there is a highest wavenumber of interest $\kappa_{1,\,max}$ (or, the smallest wavelength of interest: $\lambda_{1,\min} = 2\pi/\kappa_{1,\max}$). If the condition (34) is satisfied, the discretized spatial information (i.e., numerical dispersion relations using a_1) can satisfactorily represent the spectral behavior of the continuous periodic spatial function up to the smallest wavelength of interest. In other words, as long as the unit cell configuration meets the criterion (34), the employed FE model is adequate to capture the spectral behavior of layered composites subjected to a harmonic excitation with a long wavelength, which is greater than $\lambda_{1,\min}$.

This argument about spatial aliasing naturally leads to the effective modulus theory for dynamic problems of layered composites (Postma, 1955; Rytov, 1956). In the effective modulus theory, a layered composite is assumed to behave as a transversely isotropic continuum as long as the layer thicknesses are sufficiently small compared to the wavelength of a harmonic excitation. The five independent effective elastic moduli corresponding to the considered layered composite can be obtained within the framework of statics (Postma, 1955) or dynamics (Rytov, 1956). Moreover, propagation velocities obtained from those effective elastic moduli characterize wave motion in layered composites. If the wavelength of a harmonic excitation is smaller than $\lambda_{1,\min}$ (or, if the wavenumber of a harmonic excitation is larger than $\kappa_{1,\max}$), the effective modulus theory applied in the sagittal plane deviates from the true wave

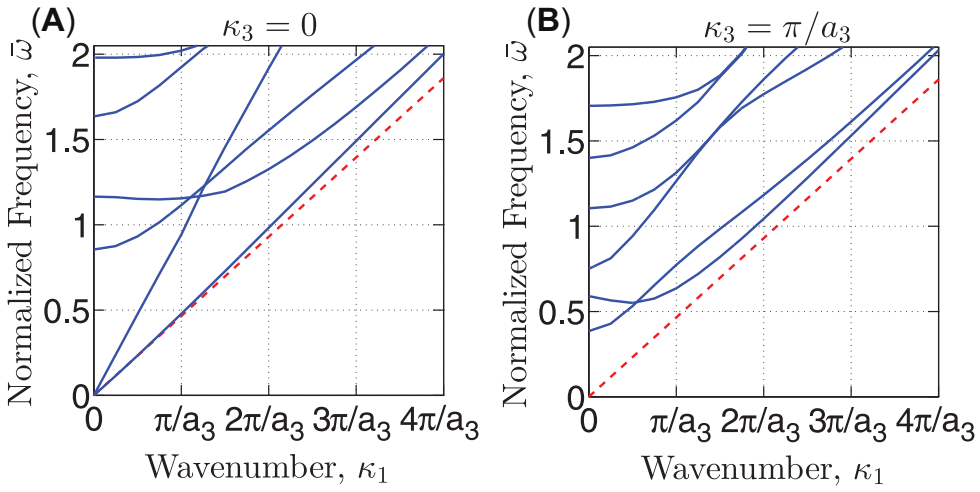

Fig. 5. Analytical dispersion relations in the direction parallel to the layers. The solid lines indicate the sagittal plane wave solution (31) with $\kappa_3 = 0$ (A) and $\kappa_3 = \pi/a_3$ (B). Note that these graphs show that wave motion in layered composites contains infinitely large κ_1 components. Moreover, the dotted lines denote the linear approximation for the frequency-wavenumber relation based on the effective modulus theory.

motion beyond a frequency $\omega_{1,\max}$:

$$\omega_{1,max} \simeq \frac{2\pi\,\bar{c}_s}{\lambda_{1,min}} = \bar{c}_s \kappa_{1,max} \tag{35}$$

where the effective shear wave velocity $\bar{c}_s$ in the sagittal plane is defined using the effective mass density $\bar{\rho}$ and the effective elastic constant $\bar{c}_{44}$ as:

$$\bar{c}_s = \sqrt{\frac{\bar{c}_{44}}{\bar{\rho}}} \quad , \quad \bar{\rho} = \frac{d\rho + d'\rho'}{d + d'} \quad , \quad \bar{c}_{44} = \frac{\mu\mu'(d + d')}{\mu d + \mu' d'} \tag{36}$$

Here, the bar notation $\bar{\cdot}$ denotes the effective quantities of the considered layered composite. Note that (35) employs the effective shear wave velocity because the lowest fictitious wave modes always comes from shear waves rather than from pressure waves (Sun et al., 1968b). Moreover, for the direction parallel to the layers (i.e., $\kappa_3 = 0$ and π/a_3), the dotted lines in Fig. 5 show the linear frequency-wavenumber relation based on the effective modulus theory.

Now, combining the anti-aliasing condition (34) and the limit condition for the effective elastic modulus theory (35), one can determine an adequate unit cell size a_1 for the highest frequency of interest ($\omega_{1,\max}$):

$$a_1 < \frac{2\pi\ \bar{c}_s}{\omega_{1,max}} \tag{37}$$

By paraphrasing, the numerical dispersion relations employing a unit cell of $a_1 \times a_3$ for the layered composite shown in Fig. 1A properly captures the true spectral behavior up to $\omega_{1,\max}$:

$$\omega_{1,max} < \frac{2\pi\ \bar{c}_s}{a_1} = \frac{2\pi}{a_1}\sqrt{\frac{\mu\mu'(d + d')^2}{(d\rho + d'\rho')(d\mu + d'\mu')}} \tag{38}$$

For the three different unit cell configurations considered in Section 3, the suggested guideline (38) is illustrated in Figs. 2D, 3D and 4D, where the maximum valid frequency $\omega_{1,\max}$ are denoted by a black horizontal line with squares. For the considered unit cell configurations, it is observed that all the fictitious modes from spatial aliasing are located above the maximum valid frequency $\omega_{1,\max}$ from (38). Furthermore, the frequency limit suggested by (38) is conservative because the 'true' shear wave velocity in layered composites is getting larger than the 'effective' shear wave velocity as the wavenumber κ_1 increases (Sun et al., 1968b) as shown in Fig. 5. This fact can be also confirmed in Figs. 2D, 3D and 4D where the gap between the frequency limit from (38) and the first fictitious modes increases as the aspect ratio $a_1/a_3 = \pi/(\kappa_{1,f} a_3)$ decreases. Thus, the results shown in Figs. 2D, 3D and 4D demonstrate the validity of the proposed guideline (38) based on the anti-aliasing condition and the effective modulus approach, and one can employ the guideline to determine a proper unit cell configuration for numerical dispersion relations for waves perpendicular to the composite layers.

Lastly, it needs to be mentioned that our proposed linear guideline is valid for the cases where researchers investigate the evolution of dispersion relations during nonlinear deformation. As mentioned in Section 1, the evolution of dispersion relations has been typically investigated in a two-step manner: static analysis in the first step and linear perturbation analysis in the second step. The results of our study contribute to the second step. In other words, the base configuration for the linear perturbation analysis is affected by the nonlinear static analysis, but the linear perturbation analysis to calculate dispersion relations is not affected. Thus, the aliasing guideline proposed in the linear context is still valid as long as elastic modulus is replaced by tangent modulus and the initial aspect ratio of an unit-cell is updated by the deformed aspect ratio.

5. Conclusion

In this paper, layered composites have been investigated as a representative example to study potential spectral distortion in dispersion relations obtained in the conventional FE framework. We have discussed and resolved the long standing issue of the spectral distortions induced by an artificial periodicity in the FE model of layered composites. Using the analytical solution for the sagittal plane waves, the fictitious modes induced from artificial finite periodicity in the direction parallel to the layers are proven to be spatial aliasing in the wavevector domain. In order to remove the spatial aliasing-induced fictitious modes in numerical dispersion relations for waves perpendicular to the layers, we propose the definitive guideline for a proper unit cell configuration. The guideline is based on the anti-aliasing condition and the effective elastic modulus theory for layered composites, and its validity is demonstrated. This study focuses on numerical spectral distortion observed in the conventional FE framework. However, its origin and the suggested guideline is universal, so they can be adopted for other numerical techniques where special discretization has to be

employed for the modeling of layered composites. Furthermore, a similar type of numerical spectral distortions can be potentially observed in the dispersion relations of periodic structures whose FE model possesses an artificial periodicity. Thus, we expect that researchers using the conventional FE method for dispersion analysis are alerted to the potential spectral distortions in the numerical results.

6. Conflict of interests

All the authors declare that there is no conflict of interest with any financial organization regarding the material discussed in this paper.

Acknowledgements

This work has been partially supported by the UB start-up funding to J. Shim.

Appendix

This Appendix briefly summarizes the solution procedure for the eigenvalue problem presented in the reference by Rouhani et al. (1983), and its specialization for $\kappa_1 = 0$. The dispersion relations of layered composites in the sagittal plane can be obtained by solving the eigenvalue problem shown in Section 2.2.2:

$$\mathbf{T}_2\mathbf{V}_n = e^{i\kappa_3 a_3}\mathbf{V}_n. \tag{31}$$

for a given κ_1. If the eigenvalue is denoted by $\lambda = e^{i\kappa_3 a_3}$, then the characteristics equation of (31) can be obtained as follows:

$$\left(\lambda^2 - 2f_1\lambda + 1\right)\left(\lambda^2 - 2f_2\lambda + 1\right) = 0 \tag{A.1}$$

where f_1 and f_2 depend on the components of the transfer matrix $\mathbf{T}_2$, i.e., T_{rs} for $r, s = 1, 2, 3, 4$. Specifically, they read:

$$f_1 = \frac{1}{2}\left[(T_{11} + T_{22}) + \sqrt{(T_{11} - T_{22})^2 + 4T_{12}T_{21}}\right]$$

$$f_2 = \frac{1}{2}\left[(T_{11} + T_{22}) - \sqrt{(T_{11} - T_{22})^2 + 4T_{12}T_{21}}\right] \tag{A.2}$$

where we employ the dependence among the components T_{rs}, i.e., $T_{33} = T_{11}$, $T_{44} = T_{22}$, $T_{34} = -T_{21}\alpha_l\alpha_t/\kappa_1^2$, and $T_{43} = -T_{12}\kappa_1^2/(\alpha_l\alpha_t)$ (Rouhani et al., 1983). Due to the symmetry of wave motions along $\kappa_3 = 0$, the four solutions (i.e., λ_1, λ_1', λ_2, λ_2') of the characteristic Eq. (A.1) satisfy the following conditions:

$$\lambda_1' = 1/\lambda_1, \quad \lambda_2' = 1/\lambda_2. \tag{A.3}$$

Then, two eigenvalues λ_m and λ_m' (here, $m = 1$ or 2) can be obtained by solving:

$$\lambda^2 - 2f_m\lambda + 1 = 0. \tag{A.4}$$

Now, the substitution of $\lambda = e^{i\kappa_3 a_3}$ provides:

$$e^{i\kappa_3 a_3} - 2f_m + e^{-i\kappa_3 a_3} = 0 \qquad \text{for} \qquad m = 1, 2. \tag{A.5}$$

After applying the trigonometric relation in (A.5), we find the dispersion relations of layered composites in the sagittal plane:

$$\cos(\kappa_3 a_3) = f_m \qquad \text{for} \qquad m = 1, 2. \tag{A.6}$$

For a fixed value of κ_1, the relation between κ_3 and ω can be obtained from (A.6). By sweeping κ_1 within the range of $(0, \infty)$, the complete picture of dispersion relations for the sagittal plane waves can be determined over the $\kappa_3 - \kappa_1$ plane.

Note that the dispersion relations of waves motion perpendicular to the layers (i.e., (21), (22)) can be easily recovered from the above sagittal plane solution. Setting $\kappa_1 = 0$ in (A.2), we obtain substantially simplified expressions for f_1 and f_2:

$$f_1 = T_{11} = \cosh(\alpha_L d)\cosh\left(\alpha_L' d'\right) + \frac{1}{2}\left(\frac{c_{11}'^2 c_p^2 + c_{11}^2 c_p'^2}{c_{11}c_{11}'c_p c_p'}\right)\sinh(\alpha_L d)\sinh\left(\alpha_L' d'\right),$$

$$f_2 = T_{22} = \cosh(\alpha_T d)\cosh\left(\alpha_T' d'\right) + \frac{1}{2}\left(\frac{c_{44}'^2 c_s^2 + c_{44}^2 c_s'^2}{c_{44}c_{44}'c_s c_s'}\right)\sinh(\alpha_T d)\sinh\left(\alpha_T' d'\right). \tag{A.7}$$

Applying $c_p = \sqrt{c_{11}/\rho}$, $c_s = \sqrt{c_{44}/\rho}$, $c_p' = \sqrt{c_{11}'/\rho'}$, $c_s' = \sqrt{c_{44}'/\rho'}$ and the hyperbolic trigonometric relations in (A.7), the decoupled analytical dispersion relations (21) and (22) can be recovered from (A.6).

References

ABAQUS Standard Analysis User's Manual Version 6.12. ABAQUS Inc., Pawtuchet, RI, USA.

Aberg, M., Gudmundson, P., 1997. The usage of standard finite element codes for computation of dispersion relations in materials with periodic microstructure. J. Acoust. Soc. Am. 102 (4), 2007–2013.

Ashcroft, N.W., Mermin, N.D., 1976. Solid State Physics. Saunders College, Philadelphia.

Babaee, S., Shahsavari, A.S., Wang, P., Picu, R.C., Bertoldi, K., 2015a. Wave propagation in cross-linked random fiber networks. Appl. Phys. Lett. 107 (21), 211904.

Babaee, S., Wang, P., Bertoldi, K., 2015b. Three-dimensional adaptive soft phononic crystals. J. Appl. Phys. 117 (24), 244903.

Bartoli, I., Marzani, A., Scalea, F.L., Viola, E., 2006. Modeling wave propagation in damped waveguides of arbitrary cross-section. J. Sound Vib. 295 (3–5), 685–707.

Bayat, A., Gordaninejad, F., 2014. A magnetically field-controllable phononic crystal. Active Passive Smart Struct. Integr. Syst. 9057, 905713.

Bayat, A., Gordaninejad, F., 2015. Dynamic response of a tunable phononic crystal under applied mechanical and magnetic loadings. Smart Mater. Struct. 24 (6), 065027.

Bertoldi, K., Boyce, M.C., 2008a. Mechanically triggered transformations of phononic band gaps in periodic elastomeric structures. Phys. Rev. B 77 (8), 052105.

Bertoldi, K., Boyce, M.C., 2008b. Wave propagation and instabilities in monolithic and periodically structured elastomeric materials undergoing large deformations. Phys. Rev. B 78 (18), 184107.

Bracewell, R.N., 2003. Fourier Analysis and Imaging. Kluwer Academic/Plenum Publishers, New York.

Brekhovskikh, L.M., 1980. Waves in Layered Media. Applied Mathematics and Mechanics, vol. 16, 2nd ed New York, N.Y., USA.

Brillouin, L., 1946. Wave Propagation in Periodic Structures: Electric Filters and Crystal Lattices. McGraw-Hill Book Company, Inc., New York.

Cheng, W., Gomopoulos, N., Fytas, G., Gorishnyy, T., Walish, J., Thomas, E.L., Hiltner, A., Baer, E., 2008. Phonon dispersion and nanomechanical properties of periodic 1d multilayer polymer films. Nano Lett. 8 (5), 1423–1428.

Duhamel, D., Mace, B.R., Brennan, M.J., 2006. Finite element analysis of the vibrations of waveguides and periodic structures. J. Sound Vib. 294 (1–2), 205–220.

Gavrić, L., 1994. Finite element computation of dispersion properties of thin-walled waveguides. J. Sound Vib. 173 (1), 113–124.

Graff, K.F., 1991. Wave Motion in Elastic Solids. Dover Publications, New York.

Guarin-Zapata, N., Gomez, J., 2015. Evaluation of the spectral finite element method with the theory of phononic crystals. J. Comput. Acoust. 23 (2), 1550004.

Han, L., Zhang, Y., Li, X., Jiang, L., Chen, D., 2016. Accelerated approach for the band structures calculation of phononic crystals by finite element method. Crystals 6 (1), 11.

He, J.J., Djafarirouhani, B., Sapriel, J., 1988. Theory of light-scattering by longitudinal-acoustic phonons in superlattices. Phys. Rev. B 37 (8), 4086–4098.

Hegemier, G.A., Bache, T.C., 1974. A general continuum theory with microstructure for wave propagation in elastic laminated composites. J. Appl. Mech. 41 (1), 101–105.

Hegemier, G.A., Nayfeh, A.H., 1973. A continuum theory for wave propagation in laminated composites-case 1: propagation normal to laminates. J. Appl. Mech. 40 (2), 503–510.

Herrmann, G., Achenbach, J., 1967. On dynamic theories of fiber-reinforced composites. In: 8th Structural Dynamics and Materials Conference. American Institute of Aeronautics and Astronautics. Structures, Structural Dynamics, and Materials and Co-located Conferences.

Hladky-Hennion, A.-C., 1996. Finite element analysis of the propagation of acoustic waves in waveguides. J. Sound Vib. 194 (2), 119–136.

Houillon, L., Ichchou, M.N., Jezequel, L., 2005. Wave motion in thin-walled structures. J. Sound Vib. 281 (3–5), 483–507.

Kohn, W., Krumhansl, J.A., Lee, E.H., 1972. Variational methods for dispersion relations and elastic properties of composite materials. J. Appl. Mech. 39 (2), 327–336.

Lagasse, P.E., 1973. Higher-order finite-element analysis of topographic guides supporting elastic surface waves. J. Acoust. Soc. Am. 53 (4), 1116–1122.

Langlet, P., Hladky-Hennion, A.C., Decarpigny, J.N., 1995. Analysis of the propagation of plane acoustic waves in passive periodic materials using the finite element method. J. Acoust. Soc. Am. 98 (5), 2792–2800.
Lee, E.H., Yang, H.W., 1973. On waves in composite materials with periodic structure. Soc. Ind. Appl. Math. 25 (3), 492–499.
Lee, S.M., Cahill, D.G., Venkatasubramanian, R., 1997. Thermal conductivity of sige superlattices. Appl. Phys. Lett. 70 (22), 2957–2959.
Li, J.B., Wang, Y.S., Zhang, C., 2008. Finite element method for analysis of band structures of phononic crystal slabs with archimedean-like tilings. In: IEEE International Ultrasonics Symposium, vol. 1–4, pp. 1468–1471.
Li, J.B., Wang, Y.S., Zhang, C., 2009. Finite element method for analysis of band structures of phononic crystal slabs with archimedean-like tilings. In: IEEE International Ultrasonics Symposium, pp. 1548–1551.
Li, J.B., Wang, Y.S., Zhang, C., 2012. Dispersion relations of a periodic array of fluid–filled holes embedded in an elastic solid. J. Comput. Acoust. 20 (4), 1250014.
Li, J.B., Wang, Y.S., Zhang, C., 2013. Tuning of acoustic bandgaps in phononic crystals with helmholtz resonators. J. Vib. Acoust. 135 (3), 031015.
Liang, B., Guo, X.S., Tu, J., Zhang, D., Cheng, J.C., 2010. An acoustic rectifier. Nat. Mater. 9 (12), 989–992.
Liu, Y., Gao, L.T., 2007. Explicit dynamic finite element method for band-structure calculations of 2D phononic crystals. Solid State Commun. 1548–1551.
Mace, B.R., Manconi, E., 2008. Modelling wave propagation in two-dimensional structures using finite element analysis. J. Sound Vib. 318 (4–5), 884–902.
Maldovan, M., Thomas, E.L., 2009. Periodic Materials and Interference Lithography for Photonics, Phononics and Mechanics. Wiley-VCH, Weinheim, Germany.
Manconi, E., 2008. The Wave Finite Element Method for 2-dimensional Structures. University of Parma Ph.D. thesis.
Mencik, J.M., Ichchou, M.N., 2007. Wave finite elements in guided elastodynamics with internal fluid. Int. J. Solids Struct. 44 (7–8), 2148–2167.
Minagawa, S., Nemat-Nasser, S., 1977. On harmonic waves in layered composites. J. Appl. Mech. 44 (4), 689–695.
Minagawa, S., Nematnasser, S., Yamada, M., 1981. Finite-element analysis of harmonic-waves in layered and fiber-reinforced composites. Int. J. Numer. Methods Eng. 17 (9), 1335–1353.
Mousanezhad, D., Babaee, S., Ghosh, R., Mahdi, E., Bertoldi, K., Vaziri, A., 2015. Honeycomb phononic crystals with self-similar hierarchy. Phys. Rev. B 92 (10), 104304.
Mukdadi, O.M., Datta, S.K., 2003. Transient ultrasonic guided waves in layered plates with rectangular cross section. J. Appl. Phys. 93 (11), 9360–9370.
Mukherjee, S., Lee, E., 1978. Dispersion relations and mode shapes for waves in laminated viscoelastic composites by variational methods. Int. J. Solids Struct. 14 (1), 1–13.
Murakami, H., 1985. A mixture theory for wave propagation in angle-ply laminates part 1: theory. J. Appl. Mech. 52 (2), 331–337.
Murakami, H., Akiyama, A., 1985. A mixture theory for wave propagation in angle–ply laminates part 2: application. J. Appl. Mech. 52 (2), 338–344.
Murakami, H., Maewal, A., Hegemie, G.A., 1979. Mixture theory for longitudinal wave propagation in unidirectional composites with cylindrical fibers of arbitrary cross section - i: formulation. Int. J. Solids Struct. 15 (4), 325–334.
Naciri, T., Navi, P., Ehrlacher, A., 1994. Harmonic wave propagation in viscoelastic heterogeneous materials part i: dispersion and damping relations. Mech. Mater. 18 (4), 313–333.
Nelson, R.B., Navi, P., 1975. Harmonic wave propagation in composite materials. J. Acoust. Soc. Am. 57 (4), 773–781.
Nemat-Nasser, S., 1972. Harmonic waves in layered composites. J. Appl. Mech. 39 (3), 850–852.
Newland, D.E., 1993. An Introduction to Random Vibrations, Spectral and Wavelet Analysis, 3rd ed Loongman, Mineola, N.Y., USA.
Nougaoui, A., Rouhani, B.D., 1987. Elastic waves in periodically layered infinite and semi-infinite anisotropic media. Surf. Sci. 185 (1–2), 125–153.
Pernot, G., Stoffel, M., Savic, I., Pezzoli, F., Chen, P., Savelli, G., Jacquot, A., Schumann, J., Denker, U., Monch, I., Deneke, C., Schmidt, O.G., Rampnoux, J.M., Wang, S., Plissonnier, M., Rastelli, A., Dilhaire, S., Mingo, N., 2010. Precise control of thermal conductivity at the nanoscale through individual phonon-scattering barriers. Nat. Mat. 9 (6), 491–495.
Petersen, D.P., Middleton, D., 1962. Sampling and reconstruction of wave-number-limited functions in n-dimensional euclidean spaces. Inf. Control 5, 279–323.
Postma, G.W., 1955. Wave propagation in a stratified medium. Geophysics 20 (4), 780–806.
Rouhani, B.D., Dobrzynski, L., Duparc, O., Camley, R., Maradudin, A., 1983. Sagittal elastic waves in infinite and semi-infinite superlattices. Phys. Rev. B 28 (4), 1711–1720.
Rytov, S.M., 1956. Acoustical properties of a thinly laminated medium. Sov. Phys. Acoust. 2 (1), 68–80.
Saini, G., Pezeril, T., Torchinsky, D.H., Yoon, J., Kooi, S.E., Thomas, E.L., Nelson, K.A., 2011. Pulsed laser characterization of multicomponent polymer acoustic and mechanical properties in the sub-GHZ regime. J. Mater. Res. 22 (3), 719–723.
Sapriel, J., Rouhani, B.D., 1989. Vibrations in superlattice. Surf. Sci. Rep. 10 (4–5), 189–275.
Shim, J., Wang, P., Bertoldi, K., 2015. Harnessing instability-induced pattern transformation to design tunable phononic crystals. Int. J. Solids Struct. 58, 52–61.
Spadoni, A., Ruzzene, M., Gonella, S., Scarpa, F., 2009. Phononic properties of hexagonal chiral lattices. Wave Motion 46 (7).
Sun, C.T., Achenbach, J.D., Herrmann, G., 1968a. Continuum theory for a laminated medium. J. Appl. Mech. 35 (3), 467–475.
Sun, C.T., Achenbach, J.D., Herrmann, G., 1968b. Time-harmonic waves in a stratified medium propagating in the direction of the layering. J. Appl. Mech. 35 (2), 408–411.
Ungureanu, B., Achaoui, Y., Enoch, S., Brûlé, S., Guenneau, S., 2016. Auxetic-like metamaterials as novel earthquake protections. EPJ Appl. Metamater. 2, 17.
Waki, Y., Mace, B.R., Brennan, M.J., 2009. Free and forced vibrations of a tyre using a wave/finite element approach. J. Sound Vib. 323 (3–5), 737–756.
Wang, P., Bertoldi, K., 2012. Mechanically tunable phononic band gaps in three--dimensional periodic elastomeric structures. Int. J. Solids Struct. 49 (19–20), 2881–2885.
Wang, P., Shim, J.M., Bertoldi, K., 2013. Effects of geometric and material nonlinearities on tunable band gaps and low-frequency directionality of phononic crystals. Phys. Rev. B 88 (1).
Wang, Y., Song, W., Sun, E., Zhang, R., Cao, W., 2014. Tunable passband in one-dimensional phononic crystal containing a piezoelectric 0.62pb(mg1/3nb2/3)o30.38pbtio3 single crystal defect layer. Physica E Low Dimens. Syst. Nanostruct. 60, 37–41.
Xu, Y.L., Tian, X.G., Chen, C.Q., 2012. Band structures of two dimensional solid/air hierarchical phononic crystals. Physica B Condens. Matter 407 (12), 1995–2001.
Zhang, Q., Zhang, K., Hu, G.K., 2016. Smart three-dimensional lightweight structure triggered from a thin composite sheet via 3D printing technique. Sci. Rep. 6, 22431.
Zhao, Y.P., Wei, P.J., 2009. The band gap of 1d viscoelastic phononic crystal. Comput. Mater. Sci. 46 (3), 603–606.